

**Key Points:**

- Synthesis data set reveals characteristic sea ice light transmittance distributions over the annual cycle
- Retrieved bulk extinction coefficients vary with progression of the season
- Parameters used in global models need careful choice while ice thickness alone is a poor predictor of light transmittance

Correspondence to:

C. Katlein,
christian.katlein@awi.de

Citation:

Katlein, C., Arndt, S., Belter, H. J., Castellani, G., & Nicolaus, M. (2019). Seasonal evolution of light transmission distributions through Arctic sea ice. *Journal of Geophysical Research: Oceans*, 124. <https://doi.org/10.1029/2018JC014833>

Received 3 DEC 2018

Accepted 10 JUL 2019

Accepted article online 16 JUL 2019

Seasonal Evolution of Light Transmission Distributions Through Arctic Sea Ice

Christian Katlein¹ , Stefanie Arndt¹ , H. Jakob Belter¹ , Giulia Castellani¹ , and Marcel Nicolaus¹

¹Alfred-Wegener-Institut Helmholtz-Zentrum für Polar- und Meeresforschung, Bremerhaven, Germany

Abstract Light transmission through sea ice is a critical process for energy partitioning at the polar atmosphere-ice-ocean boundary. Transmission of sunlight strongly impacts sea ice melting by absorption, as well as heat deposition, and primary productivity in the upper ocean. While earlier observations relied on a limited number of point observations, the recent years have seen an increase in spatially distributed light measurements underneath sea ice using remotely operated vehicles covering a wide range of ice conditions. These measurements allow us to reconstruct the seasonal evolution of the spatial variability in light transmission. Here we present measurements of sea ice light transmittance distributions from 6 years of Arctic under-ice remotely operated vehicle operations. The data set covers the entire melt period of Central Arctic sea ice. Data are combined into a pseudo time series describing the seasonal evolution of the spatial variability of sea ice optical properties from spring to autumn freezeup. In spring, snowmelt increases light transmission continuously, until a secondary mode originating from translucent melt ponds appears in the histograms of light transmittance. This secondary mode persists long into autumn, before snowfall reduces overall light levels again. Comparison to several autonomous time series measurements from single locations confirms the detected general patterns of the seasonal evolution of light transmittance variability. This also includes characteristic spectral features caused by biological processes at the ice underside. The results allow for the evaluation of three different light transmittance parameterizations, implying that light transmission in current ice-ocean models may not be accurately represented on large scales throughout all seasons while ice thickness alone is a poor predictor of light transmittance.

Plain Language Summary The interaction of sunlight with sea ice is an important key to the understanding of Arctic climate. The amount of sunlight penetrating through the ice is strongly dependent on ice and snow thickness. Optical properties of ice and snow change throughout the season. Also, sea ice properties, such as ice thickness, the cover by snow, or melt ponds are drastically changing within a few meters. To investigate the effect of these differences, we use an underwater robot to acquire high-resolution light measurements under Arctic sea ice. This enables us to describe the variations of optical properties of sea ice during the seasonal cycle. On the basis of a compilation of data from multiple expeditions, we discuss how current parameterizations in climate models need to be adapted to correctly describe the amount of light present under sea ice.

1. Introduction

Partitioning of incident solar shortwave radiation plays a crucial role for the energy fluxes across the atmosphere-sea ice-ocean boundary in polar regions. Due to the ongoing changes of the physical properties of Arctic sea ice (Meier et al., 2014), such as an increasingly younger (Maslanik et al., 2007) and respectively thinner ice cover (Haas et al., 2008; Renner et al., 2014), more sunlight is penetrating the sea ice (Nicolaus et al., 2012) causing melt and warming of the upper Arctic Ocean (Perovich et al., 2007; Steele et al., 2010). Apart from the impact on the physical climate system, light transmission through the geometrically complex sea ice cover (Katlein et al., 2016) determines the amount of energy available for in- and under-ice primary production and thus has significant impacts on the Arctic ecosystem (Assmy et al., 2017; Fernández-Méndez et al., 2015). Timing of the seasonal progression in light transmission especially in the shoulder seasons of spring and autumn can have a significant impact on annual energy budgets (Arndt & Nicolaus, 2014; Flocco et al., 2015; Perovich et al., 2017; Schröder et al., 2014) indicating the need for a better understanding of spring and autumn sea ice processes.

Light transmission through sea ice has been studied throughout the last decades (Grenfell et al., 2006; Light et al., 2008), but observations are still sparse especially when considering spatial and temporal variability of ice optical properties. Most studies have been based on point measurements (Mobley et al., 1998; Perovich et al., 1998) or short transect lines (Nicolaus et al., 2013; Perovich, 1990), as the access to the ice underside is difficult because access holes need to be drilled for every data point. The increased use of remotely operated vehicles (ROVs) under sea ice provides a better access to the ice underside (Katlein et al., 2017; Nicolaus & Katlein, 2013), allowing for spatially extensive surveys of ice optical properties in dense Arctic and Antarctic ice covers (Arndt et al., 2017; Katlein et al., 2015). In contrast to point measurements, these observations allow for a better understanding of spatial variability and the associated length scales. While autonomous and manned drifting observatories can provide valuable data on the temporal evolution of ice optical properties (Light et al., 2008; Nicolaus, Gerland, et al., 2010; C. Wang, Granskog, et al., 2014), they mostly provide a limited picture of the spatial variability in the context of the temporal evolution.

Seasonal parameterizations of light transmission through sea ice have so far been deducted from the temporal evolution of the changing physical properties of the ice cover (Arndt & Nicolaus, 2014; Perovich et al., 2011). Many model parameterizations derive light transmission from ice and snow thickness in combination with the inherent optical properties of all constituents (Holland et al., 2011; Light et al., 2003), while others solely rely on a description of seasonal melt progression (Arndt & Nicolaus, 2014). Specialized sea ice models can afford complex radiative transfer schemes, while simpler parameterizations such as the exponential model of Grenfell and Maykut (1977) are needed for large-scale circulation models due to limitations in computing time. While simplified models of sea ice light transmission certainly fall short of state-of-the-art radiative transfer models, we here want to investigate how they perform in comparison to a large-scale observational data set.

The objective of this study is to characterize the seasonal evolution of spatial variability in light transmittance through Arctic sea ice from June to October. This characterization describes the occurring spatial variability using distribution functions for individual months and characteristic phases of sea ice and surface conditions including the crucial shoulder seasons from spring to autumn. The work is based on spatially extensive measurements of Arctic sea ice optical properties, covering a large regional extent. The data set covers the seasonal melt and refreeze cycle on the basis of a large number of ROV-based observations during sea ice station work. The presented data are used to evaluate uncertainties of existing large-scale parameterizations. Results indicate how the spatial variability of light transmission varies throughout the Arctic from late winter to midautumn and how this variability needs to be accounted for by adjusting parameters in large-scale parameterizations.

2. Methods

2.1. Field Measurements

Measurements were carried out during six expeditions of the German research icebreaker RV *Polarstern* to the Central Arctic in the years 2011, 2012, 2014, 2015, 2016, and 2017. Table 1 provides an overview of the expedition dates and Figure 1 shows the respective cruise tracks. While the expeditions in the years 2011 and 2012 covered the Central Arctic in August and September, the expeditions in 2014 and 2015 covered the westerly and easterly Transpolar drift in the northernmost end of Fram Strait during the spring transition toward summer conditions (May to August). The 2016 expedition covered late season freezeup conditions (September/October) in the Central Arctic, while the 2017 expedition was observing the spring transition around the northern tip of Svalbard (May to July).

The observations cover a wide range of surface types, starting from floes covered completely in melting snow early in the year, over drained summer sea ice with a substantial melt pond cover, to the refreezing surface and first snow falls in autumn. Ice thickness in our data set ranges from very thin newly formed ice of only a few cm to thick multiyear ice of up to 3.5 m (see Table 2).

As data were acquired during 45 ice stations along six cruise tracks from various years instead of at a single location, this data set does not qualify as a time series in the strict meaning. However, this compilation is useful to provide a general view on the seasonal evolution of ice optical variability in the Eurasian sector of the Central Arctic. In particular, our observations describe a general progression of melt stages, while their respective exact timing varies regionally and can of course not be generalized from this data set. We compare our data set to several real time series observations obtained by autonomous spectral radiation

Table 1

Overview of the Expeditions Comprised in This Data Set

Expedition name	Expedition number	Polarstern number	Date	Cruise report	ROV-system (configuration)	# ROV stations
TransArc	ARK-XXVI/3	PS78	5 August to 7 October 2011	Schauer (2012)	V8-Sii (Alfred)	7
IceArc	ARK-XXVII/3	PS80	2 August to 8 October 2012	Boetius (2013)	V8-Sii (Ronia)	8
Aurora	ARK-XVIII/3	PS86	7 July to 3 August 2014	Boetius (2015)	Nereid-Under-Ice-HROV (WHOI)	3
Transsiz	ARK-XXIX/1	PS92	19 May to 28 June 2015	Peeken (2016)	V8-Sii (Siri)	8
Karasik	ARK-XXX/3	PS101	9 Sep to 23 Oct 2016	Boetius and Purser (2017)	M500 (BEAST)	8
Pascal/Sipca	ARK-XXXI/1	PS106	24 May to 20 July 2017	Macke and Flores (2018)	M500 (BEAST)	11

stations deployed on drifting ice floes in the same region as the described transect measurements, to ensure that our data set indeed reveals the temporal evolution of light transmittance throughout the season and not just regional differences.

2.2. Light Measurements Under Sea Ice

Spectral light transmittance through sea ice was measured using a RAMSES-ACC-VIS (TriOs GmbH, Rastede, Germany) spectroradiometer covering a wavelength range from 320–950 nm mounted on an under-ice ROV and an identical synchronous measurement above the surface for all presented data sets,

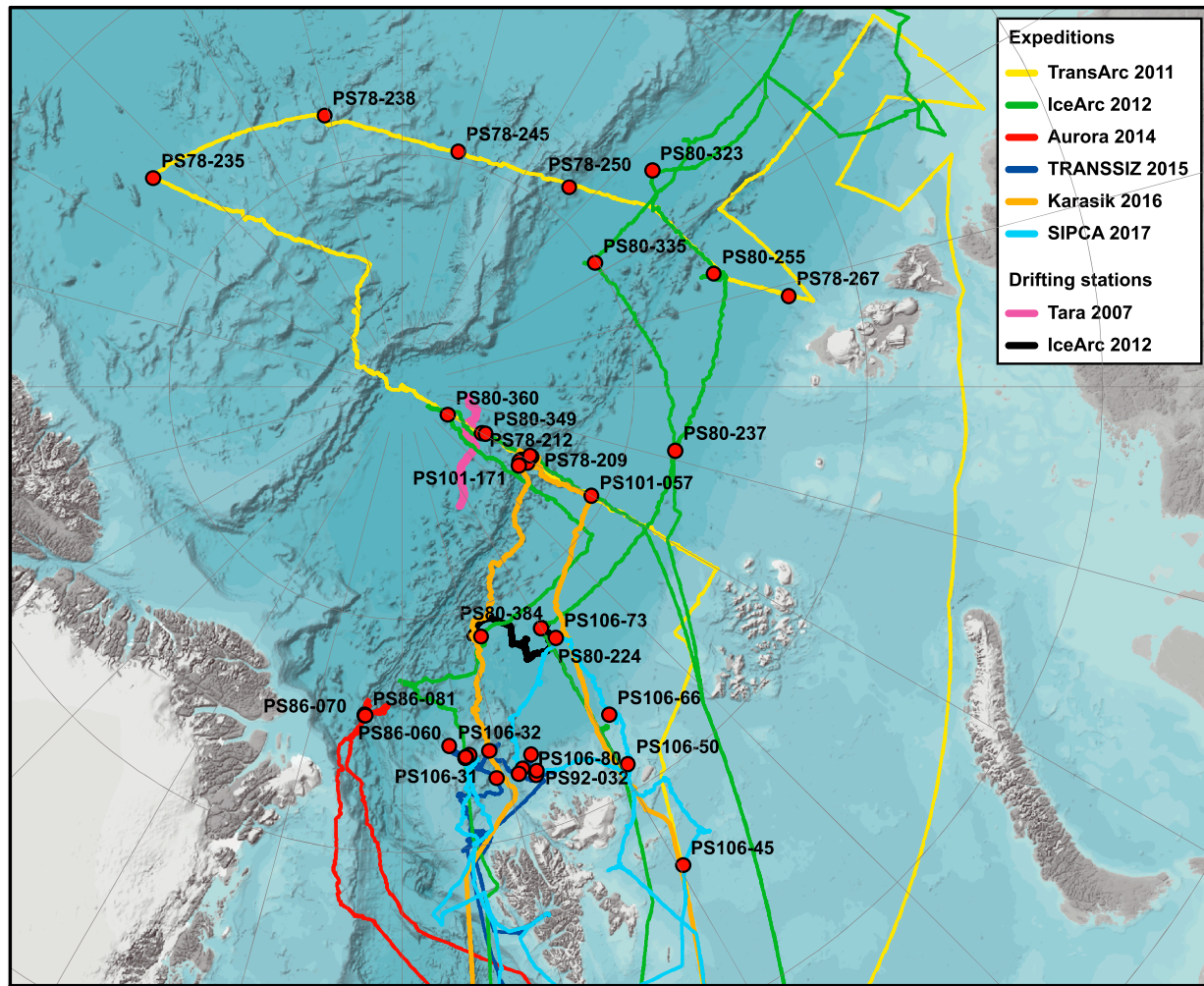


Figure 1. Map showing the cruise track of the six *Polarstern* expeditions. Positions of ice stations are indicated by the red dots. Also shown are the drift trajectories of the time series measurements at Tara close to the North Pole and during the 2012 expedition. The time series measurements during the 2017 expedition as well as several station names are omitted.

Table 2List of All ROV Stations With Characteristic Ice Draft and Light Transmittance Values as well as Its Standard Deviation σ as Available for the Analysis

Station #	Date	Latitude (°N)	Longitude (°E)	Ice type	Mean ice draft (m)	σ ice draft (m)	Mean transmittance (%)	σ transmittance (%)	Survey area (m ²)	# Spectra
PS78-209	17.08.2011	86,98	58,47	FYI	1,16	0,34	10,5	7,8	48	71
PS78-212	19.08.2011	88,01	59,97	FYI	0,98	0,60	17,6	9,2	405	481
PS78-235	03.09.2011	83,03	-130,04	NI/FYI/MYI	3,21	1,43	4,9	7,1	113	208
PS78-238	06.09.2011	83,94	-164,19	FYI	1,07	0,52	5,1	3,4	117	189
PS78-245	09.09.2011	84,79	166,42	NI/FYI	0,82	0,63	4,6	4,0	123	198
PS78-250	11.09.2011	84,39	139,93	MYI	1,00	0,45	5,7	4,0	21	31
PS78-267	17.09.2011	81,45	103,21	MYI	1,95	0,68	2,5	2,4	107	173
PS80-224	10.08.2012	84,00	30,00	FYI	1,42	0,83	7,4	7,2	492	1,183
PS80-237	16.08.2012	83,95	76,86	FYI/MYI	2,17	2,17	3,7	3,9	1,430	2,645
PS80-255	21.08.2012	82,86	109,86	FYI	0,61	0,21	8,7	6,0	207	249
PS80-323	05.09.2012	82,88	130,76	FYI	0,83	0,36	2,2	1,9	975	1,865
PS80-335	08.09.2012	85,06	122,52	FYI	0,85	0,58	2,7	3,2	1,476	2,041
PS80-349	19.09.2012	87,93	60,95	MYI	1,76	1,15	1,5	2,1	464	719
PS80-360	22.09.2012	88,83	58,53	MYI	1,11	0,35	0,9	0,9	760	1,165
PS80-384	29.09.2012	84,35	17,73	FYI	1,22	0,51	1,3	1,1	303	408
PS86-060	23.07.2014	82,90	-6,40	FYI	1,66	1,06	1,1	4,3	120	580
PS86-070	26.07.2014	82,88	-6,39	FYI/MYI	2,46	1,42	0,9	1,4	2,061	8,618
PS86-081	28.07.2014	82,88	-6,32	FYI/MYI	1,60	0,63	2,4	1,7	406	4,340
PS92-019	28.05.2015	81,17	19,13	FYI	1,17	0,24	0,4	1,6	971	2,612
PS92-027	31.05.2015	81,39	17,59	MYI	1,33	0,53	0,3	0,7	919	2,366
PS92-031	04.06.2015	81,62	19,45	FYI	1,22	0,54	1,1	2,9	1,293	3,866
PS92-032	07.06.2015	81,24	19,43	FYI	1,14	0,19	0,2	0,1	838	2,276
PS92-039	12.06.2015	81,94	13,57	FYI	1,94	1,28	0,5	1,0	245	492
PS92-043	15.06.2015	82,21	7,59	FYI	1,64	0,92	0,6	2,4	914	2,502
PS92-046	18.06.2015	81,89	9,73	FYI	1,40	0,33	3,7	2,9	1,435	3,966
PS92-047	20.06.2015	81,34	13,61	FYI	1,39	0,62	3,1	2,6	523	2,454
PS101-057	15.09.2016	85,28	60,17	FYI	0,56	1,11	19,8	10,1	518	1,217
PS101-096_1	19.09.2016	86,81	61,65	FYI	0,92	1,08	2,8	2,0	688	1,293
PS101-114_1	21.09.2016	86,99	57,74	FYI	2,25	2,50	1,8	2,9	891	1,292
PS101-114_2	21.09.2016	86,99	57,74	FYI	1,01	4,72	0,9	0,8	266	342
PS101-142_1	26.09.2016	86,84	58,21	FYI	1,10	1,10	0,9	0,7	1,466	2,090
PS101-142_2	26.09.2016	86,84	58,21	FYI	0,75	0,82	1,2	1,1	257	374
PS101-162	29.09.2016	86,96	56,01	FYI	0,91	5,61	1,4	2,7	1,211	1,620
PS101-171	01.10.2016	86,86	61,66	FYI	0,77	1,09	2,1	2,8	698	896
PS106-25	08.06.2017	81,91	9,87	FYI	0,59	0,86	4,3	2,8	1,499	3,268
PS106-27	10.06.2017	81,90	10,23	FYI	0,58	1,04	7,3	4,3	1,420	4,263
PS106-28_1	10.06.2017	81,87	10,74	FYI	1,04	1,91	8,7	4,9	867	1,792
PS106-28_2	11.06.2017	81,87	10,74	FYI	0,53	0,64	6,4	4,2	1,332	3,321
PS106-31	14.06.2017	81,80	11,28	FYI	0,76	1,52	8,6	6,0	734	3045
PS106-32	15.06.2017	81,73	10,86	FYI	0,69	1,60	9,1	4,7	931	2,924
PS106-45	25.06.2017	78,09	30,47	FYI	1,22	1,73	3,7	4,0	1,018	1,809
PS106-50	29.06.2017	80,55	30,99	FYI	1,92	2,89	8,2	2,3	1,610	3,557
PS106-66	03.07.2017	81,66	32,34	FYI	2,68	1,08	2,3	1,1	528	1,080
PS106-73	07.07.2017	83,66	31,58	FYI	1,23	5,01	7,6	7,2	2,141	5209
PS106-80	12.07.2017	81,31	16,89	FYI	1,53	2,25	16,4	11,5	737	2,007

Note. ROV = remotely operated vehicle; FYI = first year ice; MYI = multi year ice; NI = new ice. Dates are formatted as DD.MM.YYYY.

respectively. In 2011, 2012, and 2015, optical sensors were carried on board a V8Sii observation class ROV (Ocean Modules, Atvidaberg, Sweden; Nicolaus & Katlein, 2013), while in 2016 and 2017 we used a purpose-built improved M500 ROV (Ocean Modules, Atvidaberg, Sweden) as measurement platform (Katlein et al., 2017). Both used ROV systems were operated directly from the examined ice floe through an individual hole in the ice or in rare cases over the ice edge. In 2014, sensors were mounted on the Nereid Under Ice hybrid-ROV developed by the Woods Hole Oceanographic Institution in collaboration with the Johns Hopkins University (Katlein et al., 2015). The large size of the hybrid ROV

required a launch from the icebreaker for operating under the surrounding sea ice. Details about data processing, ice relative positioning and calibration have been described earlier (Katlein et al., 2015; Katlein et al., 2017; Nicolaus, Hudson, et al., 2010; Nicolaus & Katlein, 2013). Spectral measurements were integrated over the spectral range of the instruments from 320 to 950 nm for most applications in this manuscript.

During the IceArc expedition in late summer 2012, an autonomous station measuring sea ice light transmittance using several RAMSES-ARC radiometers through ponded and unponded sea ice was deployed on 11 August and recovered 48 days later on 28 September. Both, deployment and recovery of the station, were combined with additional transect measurements of the ROV. These autonomous measurements cover the time period of most dominant surface changes of Arctic sea ice, from a ponded surface toward a completely refrozen and snow-covered sea ice surface. A very similar setup was used in 2017 on the PASCAL/SIPCA expedition to measure light transmission through the spring transition from 31 May to 12 July. Here, the surface evolved from spring toward summer conditions, that is, showing a mixture of developing melt ponds and bare ice.

These time series covering the melt and freezeup period are complemented with data acquired during the drift of the ship Tara between 29 April and 4 September 2007 (Nicolaus, Gerland, et al., 2010) covering the entire summer season at a location closer to the geographic North Pole.

2.3. Data Processing

Data from all ROV campaigns was compiled, corrected for the water layer between the sensor and the ice, and quality controlled as described in Nicolaus and Katlein (2013). All data with a sensor inclination exceeding 10° and a sensor depth of more than 15 m were discarded prior to the analysis. Thus, the remaining uncertainties associated with sensor orientation are 0.3% (Nicolaus & Katlein, 2013). To remove the influence of water between the sensor and the investigated ice, all data were corrected using water extinction coefficients derived from vertical light profiles (Katlein et al., 2016; Nicolaus & Katlein, 2013). This resulted in a total of 35,642 valid spectra of under-ice irradiance and sea ice light transmittance. To avoid effects from multiple sampling of the same profile line, all data were gridded with 1-m resolution, by averaging all measurements taken within a grid cell (Katlein et al., 2014). The processed data set is available online from PANGAEA (<https://doi.pangaea.de/10.1594/PANGAEA.896219>).

Bulk extinction coefficients κ were calculated for use in the sea ice light transmission parameterization proposed by Grenfell and Maykut (1977) from sea ice transmittance T and the sea ice draft z_{draft} . Sea ice draft was measured by the difference between the ROV depth and the distance to the ice determined by sonar altimeter. According to Grenfell and Maykut (1977) the light transmitted through sea ice can be parameterized as $F_T = F_0 \cdot i_0 \exp(-\kappa \cdot z_{\text{ice}})$, with the incident irradiance F_0 , surface transmission parameter i_0 (describing the fraction of light that gets transmitted more than 10 cm below the surface), sea ice bulk-extinction coefficient κ , and the ice thickness z_{ice} . In many ice-ocean models sea ice light transmittance T is parameterized independently of explicit treatment of surface properties (Castellani et al., 2017), such as albedo or surface scattering layers as $T = F_T/F_0 = i_0 \exp(-\kappa \cdot z_{\text{ice}})$ with typical choices of $i_0 = 0.35$ and $\kappa_{\text{ice}} = 1.5 \text{ m}^{-1}$ (Perovich, 1996). Therefore, we calculated here sea ice bulk extinction coefficients as

$$\kappa = \frac{-\ln(T/i_0)}{z_{\text{draft}} \cdot b} \quad (1)$$

with $i_0 = 0.35$ and a correction factor of $b = 1.1$ converting the draft measurements to ice thickness. This rough treatment of light transmission through sea ice attributes changes in ice optical properties throughout the ice column and also particularly in the surface layer to one single extinction coefficient. While a more sophisticated treatment of radiative transfer has been achieved for point measurements (Ehn et al., 2008; Light et al., 2008; Mobley et al., 1998) and incorporated into a few specialized sea ice models (Holland et al., 2011), this simplistic treatment is mostly used in large-scale models due to limited computational resources, e.g. the MITgcm (Castellani et al., 2017). In particular, the choice of a constant value of i_0 impacts the derived extinction coefficients. A value of $i_0 = 0.35$ is representative for bare white ice under overcast skies, which is a very good assumption in most situations in the central Arctic. We use this value to be able to consistently compare to the most frequently used model parameterization.

Here we include also cases with snow cover into our analysis. The original parameterization by Grenfell and Maykut (1977) was never intended for use in snow-covered cases. Many models such as the standard configuration of MITgcm (Castro-Morales et al., 2014; Marshall et al., 1997) thus just assume zero light transmission through snow. As this is clearly not the case in our data set, we extend our evaluation into the snow-covered shoulder seasons. Equally as with variable properties of a surface scattering layer, snow cover thus results in an increased bulk extinction coefficient. While this attributes a wrong extinction coefficient to the ice, it would be the coefficient that needs to be used in a simple one layer parameterization to arrive at the right light transmittance. The original parameterization is built for broadband fluxes (400–2,500 nm), where values above 1,000 nm were obtained by extrapolation. As the parameterization has been used in models for a variety of spectral bands and the resulting bias is less than 10%, we decided not to adjust our measurements (320–950 nm) using empirical factors.

3. Results

3.1. Physical Properties of the Ice Floes

Ice stations and measurement areas were selected to be representative for the sea ice in the region at the given date. Sea ice properties of each sampled station are summarized in Table 2. Here, we sampled 41 stations on first-year ice with a mean sea ice thickness of 0.97 m, ranging between 0.22 and 2.47 m. The thickest ice was observed northeast of Greenland with a significant amount of melting snow with a modal thickness of 0.12 m surveyed in July 2014. Thinner ice, that is, nilas, was sampled in 2011 only. Only a few stations were located in multiyear ice regions in the vicinity of the North Pole and had an ice thickness of around or above 2 m. In the following, the different ice thickness of individual stations is not considered separately, as it is a poor predictor of transmittance, explaining only about 16% of the variance in this large-scale data set. This is somewhat counterintuitive but reflects the high influence of surface scattering properties and features such as ridges or melt ponds influencing light transmission.

The seasonal evolution of snow was observed as expected: In May, highest snow thicknesses of up to 0.4 m were measured, which decreased in June followed by a phase of snow free ice during August. The first snow fell on the refreezing ice at the end of August. Figure 2 shows areal images of the surveyed ice floes at the different stages of surface melt and refreezing and allows a qualitative description of the seasonal evolution of sea ice surface properties. In early June, the surface still closely resembled the winter state with a homogeneous white color and more or less spatially uniform surface albedo (Figure 2a). Toward the beginning of July, the surface got wetter, with the snow melting and the first signs of melt pond formation (Figure 2b). Toward the end of July, highest melt pond cover was reached widely (Figure 2c); however, snow cover was partially still dominant leading to melt pond formation within the snow layer. Subsequently, the surface layer drained and melt ponds retreated into a more discrete pattern (Figure 2d). In the beginning of August, almost all snow had melted and a coarse granular surface scattering layer covers the ice floes. This white surface was strongly contrasted by melt ponds colored from light to dark blue, depending on the thickness of the underlying ice (Figure 2e). Toward the end of August, when air temperatures drop below 0 °C again, a thin ice layer grows on the melt ponds, which slowly thickens during freezeup (Figure 2f). Refrozen and snow-covered ponds stay discernable for a significant time far into September (Figure 2g) until the surface characteristics get more and more uniform again, as soon as first significant snow fall events occur (Figure 2h). While we state dates for the different above mentioned melt phases in our data set, the actual timing can vary significantly in different regions and should thus rather be viewed as a progression of melt phases, than definitive dates.

This observed series of changing surface properties of Arctic sea ice is consistent with previous observations (Fetterer & Untersteiner, 1998; Nicolaus, Gerland, et al., 2010; Perovich et al., 2002; Perovich & Polashenski, 2012; Webster et al., 2015).

3.2. Seasonal Evolution of Light Transmittance

Figures 3–5 illustrate the seasonal evolution of light transmittance through Arctic sea ice. As our data set is not a time series at a fixed location, care must be taken in the interpretation and discussion of the overall results. The large number of spatially distributed observations on different sites provides, however, a much more representative picture of light transmittance through Arctic sea ice, and especially the evolution of spatial variability of ice optical properties throughout the seasonal cycle. This is supported by the comparison of

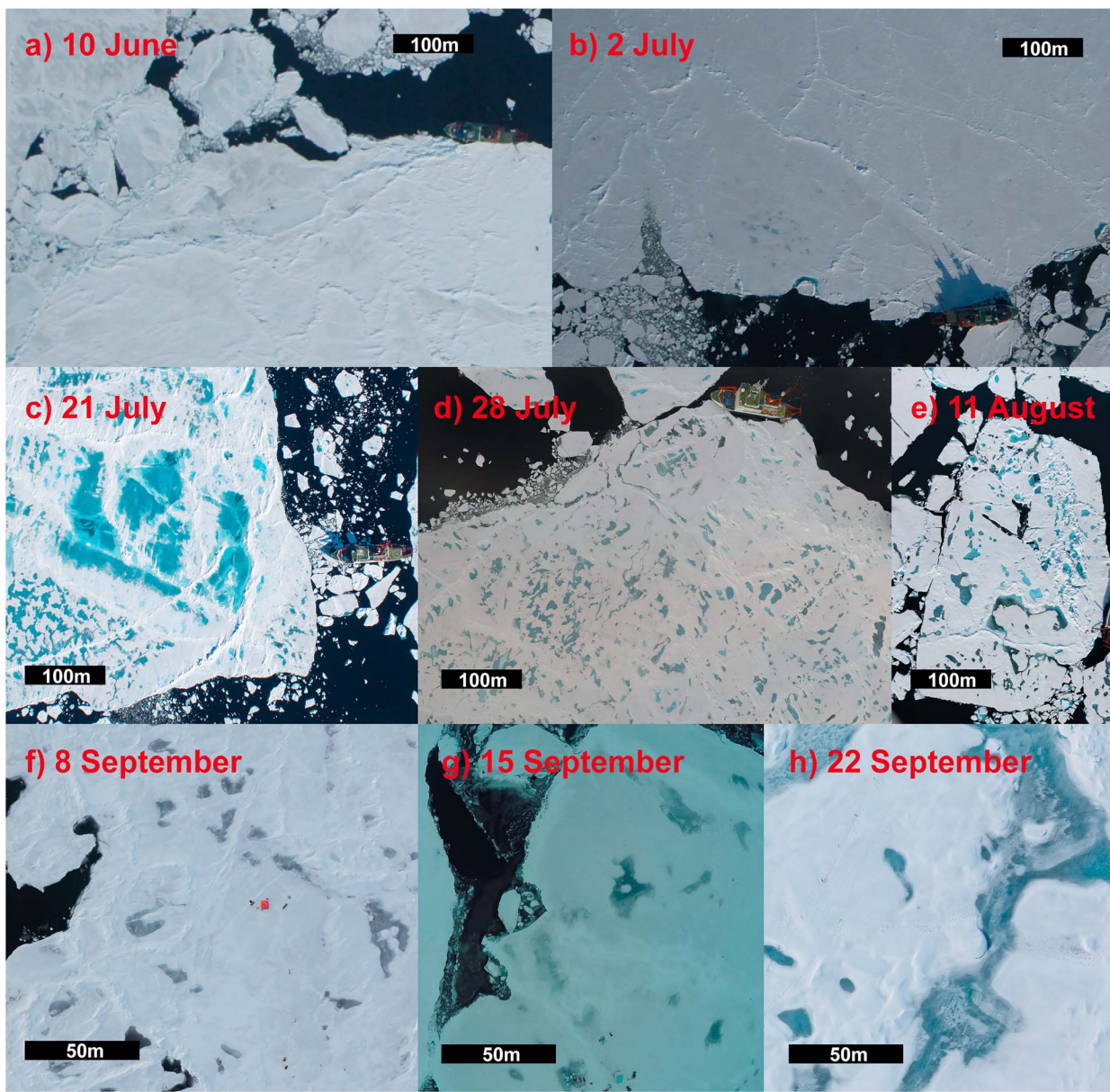


Figure 2. Aerial images showing the seasonal evolution of surface properties on selected remotely operated vehicle measurement sites from expeditions in different years: (a) early spring situation with continuous snow cover, (b) melting snow cover with initial signs of pond formation, (c) widespread surface ponding due to enhanced melt, (d and e) summer stage with mostly drained surface and more discrete pond patterns, (f) melt ponds covered with thin ice and first thin snow cover, (g) refreezing of leads and ponds, and (h) developing snow cover also on melt ponds.

our data with actual time series measurements in single locations from autonomous drifting stations during the IceArc expedition in 2012, the PASCAL/SIPCA expedition in 2017, and the Tara drift in 2007. Figure 3 presents all measured transmittance histograms from ROV measurements together with these actual time series. Figure 4 shows monthly averaged transmittance histograms, while Figure 5 depicts the seasonal evolution on the basis of selected stations.

3.2.1. Wavelength-Integrated Light Transmittance

In May, light transmittance is below 0.01. Accordingly, spatial variability is very low in this stage of the seasonal cycle. This is linked directly to the uniformity of the surface with high albedo and a significant snow cover. With wetting and melting of the snow cover, transmittance gradually increases to levels of 0.05 to 0.01. As snow melting and pond formation are both processes with great spatial heterogeneity,

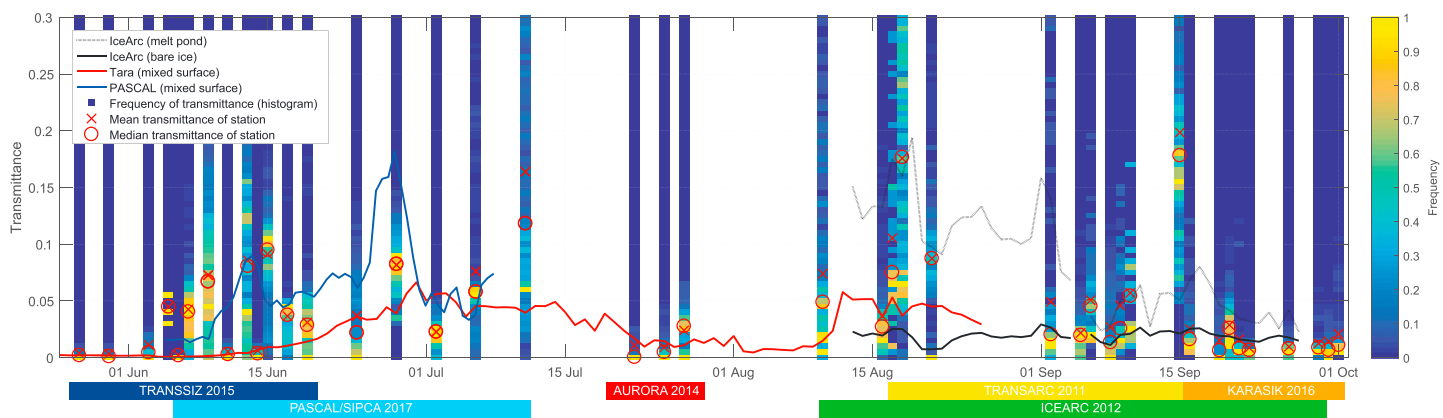


Figure 3. Pseudo time series of light transmittance through sea ice as measured through the course of the year: Normalized histograms of each station are shown, with bright colors indicating frequent occurrence of the transmittance value. Mean (crosses) and median (circles) transmittance on the respective stations are given by the red symbols. Black lines represent time series data acquired during the IceArc expedition (bare ice = solid; melt pond = dotted), the Tara drift (red line; Nicolaus, Gerland, et al., 2010), and measured by an autonomous drifting station during the PASCAL/SIPCA expedition 2017.

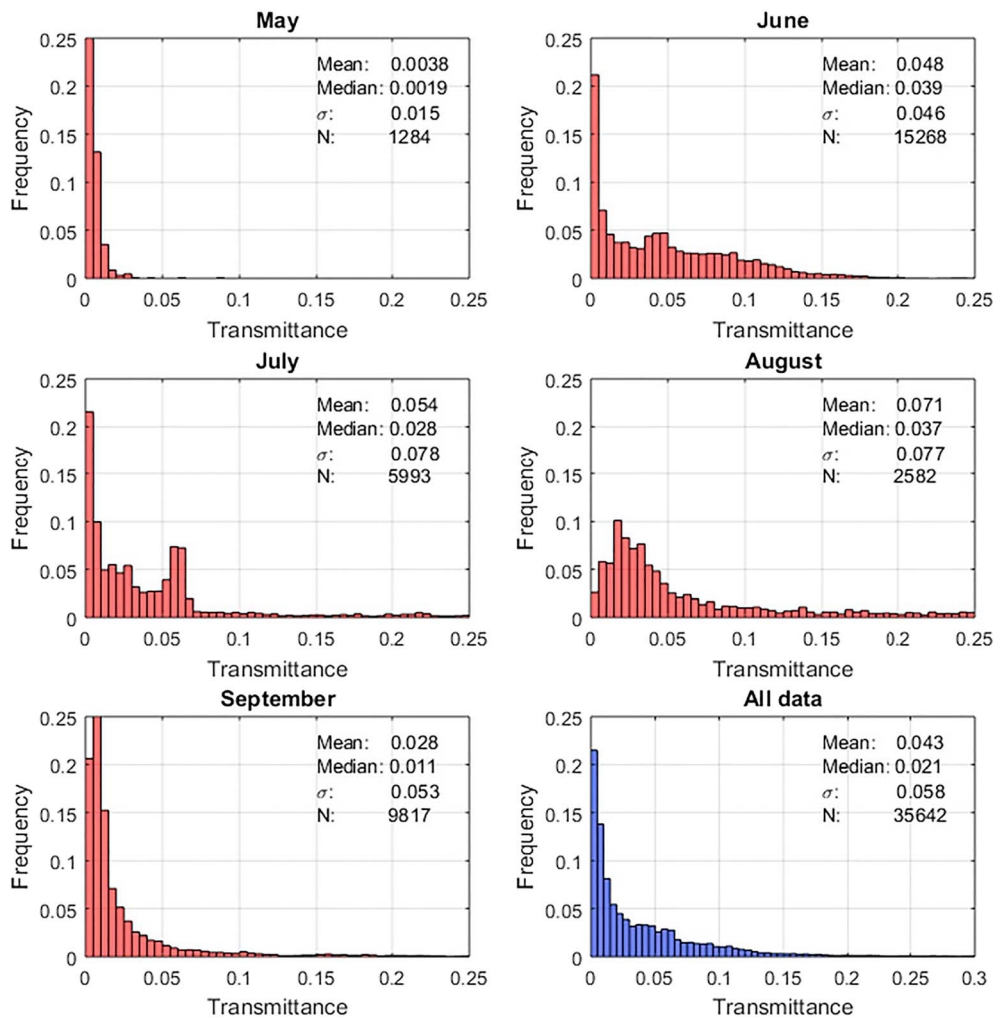


Figure 4. Histograms of sea ice light transmittance in the months May to September. Each histogram summarizes all available data from the respective month.

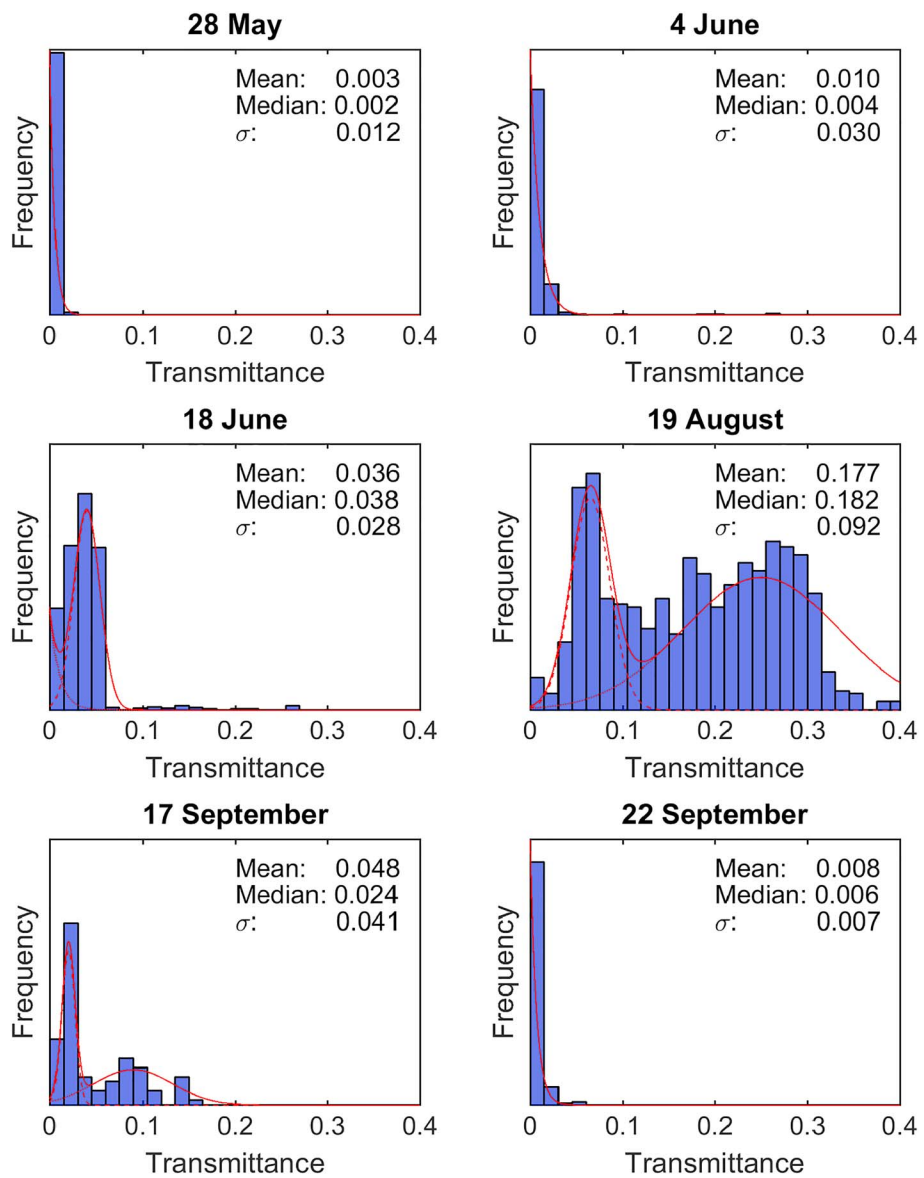


Figure 5. Histograms of sea ice transmittance at selected stations showing the general stages of seasonal development. Red lines indicate theoretical composition of the histogram (solid) as sum of the exponential distribution and Gaussian modal peaks (dotted and dashed).

the spatial variability of light transmittance is increasing gradually with progressing melt. This results in a much broader histogram than before (Figure 4b). The described spring-summer transition is of crucial importance for the annual energy budget of the Arctic Ocean, as highest solar radiation fluxes are transmitted from May to July (Arndt & Nicolaus, 2014; Arrigo et al., 2012). However, wide generalizations are difficult during this transition phase, as light transmittance greatly depends on synoptic scale events determining melt onset, the last snowfall, the sequence of pond formation, and the time when snow has completely melted (Perovich et al., 2017). These synoptic factors exhibit substantial regional and also interannual variability.

Local variations in snow depth and its spatial distribution patterns do also affect spatial variations in light transmittance of Arctic sea ice during summer. For example, the sampled area northeast of Greenland (PS86-081, 28 July 2014) reveals a relatively thick snow cover, while the averaged light transmittance is 2.4% only. In contrast, measurements from north of Svalbard (PS106-80, 12 July 2017) 1 week earlier indicate light transmittance values up to 16.4%. These observations seem to be contradictory and point to

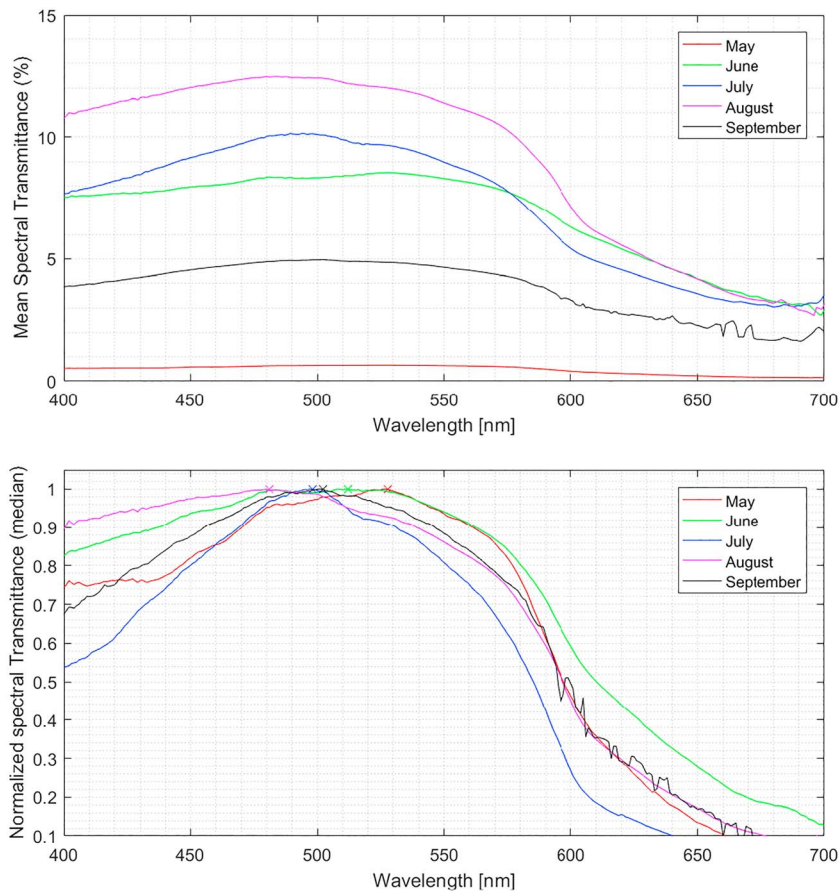


Figure 6. Mean spectral transmittance for all months from May to September. Absolute values are shown in the top panel, while the lower panel shows the spectra normalized to their maximum. The wavelength of the maximum is indicated by the cross. Spectral shape in July differs significantly from the other months, showing impact of biological absorption. Due to low absolute light levels September values above 580 nm are contaminated by noise.

strong regional differences. The strong variations in light transmittance might however also be related to temporally varying light absorption in and under Arctic sea ice. Nicolaus, Gerland, et al. (2010) discussed a comparable summer drop in the light transmittance during the Tara drift related to increasing biomass absorption. The spectral signature of the measurements of both, the Tara time series, as well as our data record, show clear evidence of ice algae by a shift in the spectral maximum transmittance, as seen in Figure 6. Also, bottom ice algal assemblages were observed with the ROV but could not be quantified.

The measurements in the first half of August show typical conditions for a well-developed melting stage of first-year sea ice. Modal bare ice transmittance values are around 0.05 to 0.07, while modal pond transmittance values reach up to 0.25, consistent with previous observations (Nicolaus et al., 2012). Single ponds show even higher transmittances. Spatial variability is highest during this phase with large variations caused by the spatial variability in both surface properties and ice thickness.

The subsequent refreezing of the surface can be roughly divided into two phases. At first, the amount of light transmittance gets reduced due to ice formation on melt ponds and the first appearing snow patches. However, the high spatial variability remains due to the patchy distribution of new snow, and the still existing contrast in the optical properties between refreezing melt ponds and the surrounding bare ice. In the second half of September, transmittance and its spatial variability decrease gradually with increasing snowfall and refreezing, homogenizing the surface and reducing transmittance again to values below 0.02 (Figure 4e).

Figure 4 shows the spatial distribution functions of light transmittance separated into monthly compositions from May to September. The monthly distribution patterns confirm the previously described “pseudo time series” of light transmittance: While the distribution widens toward higher transmittance values from

May to June, the appearance of a second modal peak reveals the initial formation of melt ponds from July onward. This long tail of the distribution toward high transmittance values encompasses a wide variety of highly translucent melt ponds with very different properties in August. As soon as snow accumulation dominates sea ice surface properties again in September, light transmittance drops while the multimodal shape of the transmittance distribution weakens or even disappears.

3.2.2. Spectral Light Transmittance

To identify changes in the spectral shape of light transmittance throughout the course of the season, we grouped all acquired spectra by month and averaged them for the entire spectral range from 320 to 950 nm (Figure 6). Overall, spectral transmittance increases from May to August. While the spectral shape is similar in May and June, a clear shift in spectral shape can be observed from June to July. Here, the leading edge of the spectrum between 400 and 500 nm becomes much steeper, indicating significant absorption in this wavelength range likely due to biomass contained in the ice. This reconfirms that the drop in light transmittance during July described above might be caused by algal absorption. In combination with earlier observations (Nicolaus, Gerland, et al., 2010), this leads us to the conclusion that a reduction in light transmittance caused by algal absorption is likely a ubiquitous feature also in the drifting pack ice of the Arctic Ocean. As soon as the ice warms, this biomass gets flushed out of the ice. Consequently, a flatter upslope of the spectrum is regained during August, the month of highest light transmittance. In September, light transmittance reduces to its June level, however, with a significantly different spectral shape. The leading edge of the spectrum is significantly steeper again, likely showing first evidence of snow absorption.

3.2.3. Seasonal Evolution of Spatial Variability

Figure 5 illustrates the spatial variability of light transmittance at selected stations throughout the seasonal cycle. During spring, when sea ice is still snow covered (28 May/4 June), the spatial variability is rather small. Thus, distribution functions can be represented by an exponential distribution with a single modal peak at the lowest transmittance and a steep decrease toward slightly higher transmittance values. Once the snow melts (18 June), the transmittance distribution shows a particular modal peak distinguished from the underlying exponential distribution associated with increasing light transmittance during this period. This pattern strengthens with increasing surface melt, involving a weakening of the underlying exponential distribution, while the modal peak develops a longer tail of higher transmittance values. With pond formation (19 June), this tail develops into a second modal peak representative of melt pond transmittance. This bimodal configuration dominates the typical histogram of light transmittance through Arctic summer sea ice as reported earlier (Nicolaus et al., 2012). This bimodal structure is however not so evident in the monthly histograms presented in Figure 4. This is caused by the high regional variability in pond properties, rather leading to a long tail of high transmittances than a second modal peak in a monthly data compilation. During freezeup, the spatial variability is retained initially, while the magnitude of transmittance in both modal peaks decreases due to snowfall and refreezing (17 September). With increasing snow accumulation on the frozen surface, the surface regains its homogeneous winter appearance (22 September). Consequently, the transmittance histogram turns into an exponential distribution again, indicating the evolution toward less spatial variability of light transmittance during this period.

The length scale of spatial variability as derived from histogram analysis (Katlein et al., 2015) does not show any seasonal trend over this large data set (not shown). This might be caused by the fact that different processes, including sea ice deformation, melt pond formation, and snow redistribution features, acted differently on each of the surveyed ice floes. As these processes tend to influence each other during the course of the season, but do not change their spatial scale of variability, the length scale of transmittance variability is expected to remain rather consistent throughout the year in a given location.

3.2.4. Extinction Coefficients

Bulk extinction coefficients were calculated from the wavelength integrated transmittance measurements following equation (1). Figure 7 shows monthly grouped histograms depicting the seasonal evolution of the optical properties of the ice cover. As sea ice thickness and snow depth measurements colocated with ROV transects are hardly available, ice draft measured by the ROV was used for calculation of the bulk extinction coefficient. Consequently, the quantitative description of variations in the sea ice surface properties, that is, snow depth, surface ponding, and properties of the surface scattering layer, is missing. This lack of accuracy needs to be taken into account, when discussing the estimated bulk extinction coefficients. In our treatment, the extinction coefficient resembles the optical properties of the entire ice column

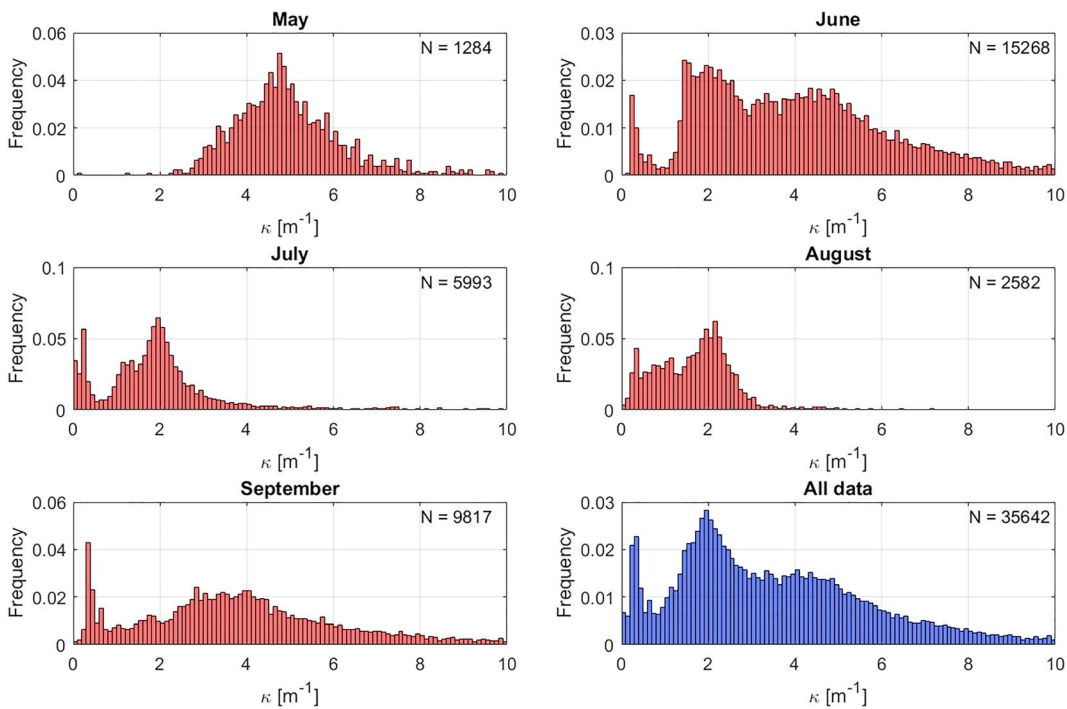


Figure 7. Monthly histograms of bulk extinction coefficients derived according to equation (1) (Grenfell & Maykut, 1977).

including a wide variety of surface properties, such as snow cover or melt ponds. However, our results can provide guidance toward the choice of extinction coefficients and their variability in simple radiative transfer parameterizations in climate models.

High values of extinction coefficients from 4 to 5 m^{-1} are frequently observed in May and September related to the prevalent snow cover. During the summer months, that is, June to August, modal peaks are located around 2 m^{-1} . While light transmittance exhibits the largest variability in August, extinction coefficients reveal the narrowest distribution function compared to the adjacent shoulder seasons. This is related to the simpler geometric properties of the bare sea ice in contrast to snow-covered surfaces. Thus, estimated summer extinction coefficients are more consistent with previously published values of in-ice extinction coefficients in the range of $0.8\text{--}1.5 \text{ m}^{-1}$ (Grenfell & Maykut, 1977; Light et al., 2008; Perovich, 1996).

4. Discussion

4.1. Bimodal Structure of Autumn Freezeup Light Transmittance

While the bimodal structure of light transmittance in ponded sea ice has been described before (Kattlein et al., 2015; Nicolaus et al., 2012), our data set shows that this bimodal structure is conserved even during the first weeks of freezeup (Figure 5), when melt ponds start to freeze over and the first snow accumulates on the surface. While this indeed lowers the absolute value of light transmittance over the entire surface, melt ponds still provide a significantly brighter window of light into the ocean than bare ice. This can have adverse effects on the thermodynamic evolution of sea ice (Flocco et al., 2015) and especially might be an energy source for late season ice algal and pelagic phytoplankton autumn blooms (Lee et al., 2011). During the freezeup period, when refreezing initiates nutrient resupplies by mixing in the surface layers of the ocean, melt ponds might be an important key element to understand the amount of under-ice biological production. While ponds are transmitting a significant portion of the diminishing daylight into the upper water column, it has to be noted that the absolute fluxes are low. Thus, the appearance of the bimodal structure in spring during the time of highest solar fluxes at the surface has a more drastic effect on the under-ice light climate.

Identifying the importance of a detailed understanding of the bimodal structure of autumn freezeup light transmittance reveals the need to describe its physical details not only on a local observational scale

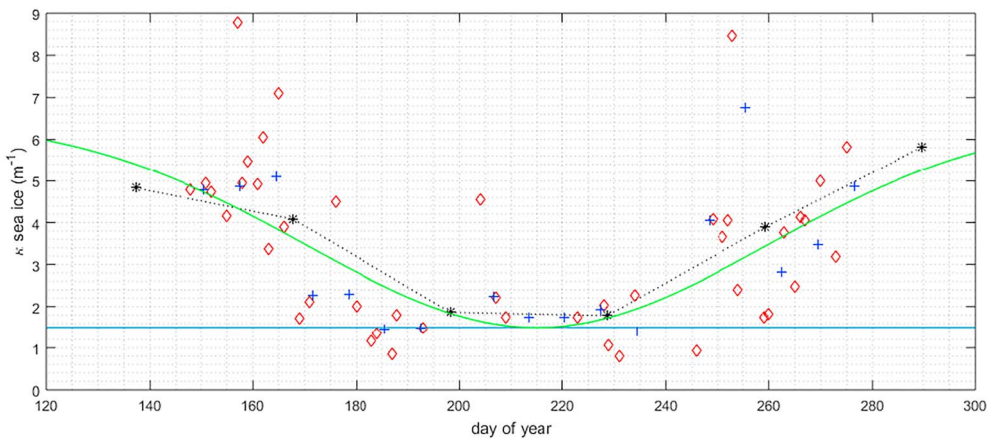


Figure 8. Median bulk extinction coefficients for each station according to the respective day of year (red diamonds). Blue crosses indicate weekly medians and black stars monthly median values. The blue solid line indicates the frequent choice of $\kappa = 1.5 \text{ m}^{-1}$ for the GM77 parameterization. The green line depicts a simple parameterization $\kappa = 6.5 - \left(5 * \exp\left(\frac{-(d-215)^2}{4000}\right)\right)$ that could be used to improve light field estimates in large-scale models as a function of d , the day of year.

(~100 m) but also on medium- (10 km) to Arctic-wide scales (1,000 km). We therefore suggest, especially for coupled large-scale models, to improve their simplified melt pond parameterization schemes based on air temperature evolution (Liu et al., 2007) by including an explicit description of surface properties, that is, forming/refreezing melt ponds and snow cover. However, the implementation in dedicated sea ice models with explicit physical melt pond parameterizations (e.g., Taylor & Feltham, 2004) and complex radiative transfer scheme (Briegleb & Light, 2007) might be more feasible.

4.2. Extinction Coefficients for Modeling

So far, optical parameters for radiative transfer models were obtained from a few point measurements (Ehn et al., 2008; Grenfell & Maykut, 1977; Light et al., 2008; Mobley et al., 1998) or laboratory analysis of ice samples (Grenfell & Perovich, 1981; Light et al., 2015). Our data set provides the possibility to evaluate the parameter choice in simple radiative transfer parameterizations on the basis of a huge variety of measurements. The advantage of this compilation from various snow and ice conditions is that it does not only represent one single case study. This helps to derive more general parameterizations because also model ice conditions mostly need to represent a broad range of conditions existing within a single grid cell.

During summer, when the influence of snow on the sea ice is minimal, the modal peak of calculated bulk light extinction coefficients lies around $\kappa = 2 \text{ m}^{-1}$. This is slightly higher than the widely used choice of $\kappa = 1.5 \text{ m}^{-1}$ in respective radiative transfer parameterizations. A second mode between 0.5 and 1.5 m^{-1} , representing melt ponds, becomes evident in the extinction coefficient histograms of July and August (Figure 7), comparable to what was described from monthly distribution functions from the light transmittance in the same time period. Consequently, we presume models using the typical extinction coefficient of $\kappa = 1.5 \text{ m}^{-1}$ throughout the year may be overestimating light transmission especially during spring and autumn. This is countering the suggestion by Light et al. (2008) to use an even smaller extinction coefficient of $\kappa = 0.8 \text{ m}^{-1}$ (Light et al., 2008). However, their value was derived using an i_0 value of 0.93 for visible light (350–700 nm) and thus cannot be directly compared to our extinction coefficients retrieved using a constant i_0 value of 0.35, as i_0 and κ values are dependent on each other. Subsequently, also light transmittance may be overestimated during spring and the freezeup period, when snow modifies sea ice surface properties. Analyzing the seasonal change in determined extinction coefficients allows us to suggest a parameterization of it as function of the day of year (Figure 8).

However, it should be noted that the parameter $i_0 = 0.35$ in the parameterization is kept constant in our analysis (equation (1)), as we do not generally have detailed knowledge about the associated surface albedos available for the entire data set. If this parameter would be varied according to season or surface

temperature as in some models, the misfit seen during the shoulder seasons in this comparison would decrease.

Due to missing colocated sea ice thickness and snow depth measurements with the presented under-ice measurements, we use only ROV-derived ice draft measurements to describe sea ice geometry. Thus, we can only evaluate the easiest exponential radiative transfer parameterization suggested by Grenfell and Maykut (1977). This parameterization is, however, widely used in many large-scale coupled simulation and forecasting systems, such as PIOMAS (Zhang & Rothrock, 2003), MITgcm (Castellani et al., 2017; Losch et al., 2010), and FESOM (Q. Wang, Danilov, et al., 2014).

More precise colocated manual measurements of ice thickness, snow thickness, melt pond depth, and properties of the surface scattering layer—as would be required for a comparison to the more complex parameterizations—are only available on a very small subset of the data set. In addition, these properties are often also poorly represented in models, making an accurate comparison difficult. In general, parameters for any parameterization should be derived from observations of the same complexity level. A better surface classification combining ROV-based ice draft measurements from multibeam sonar (Katlein et al., 2017) with surface topography derived from terrestrial laser scanning (Polashenski et al., 2012) and aerial photography will enable more complex comparisons also on similarly large data sets in the future.

4.3. Comparison to a Large-Scale Light Transmission Parameterization

A seasonal parameterization of light transmittance through Arctic sea ice based on the 2011 subset of this data set was developed by Arndt and Nicolaus (2014). Here, light transmittance is described as a function of ice type (i.e., melting/forming sea ice, seasonal, and perennial sea ice), the associated melt pond coverage and the seasonal progression of surface melt by melt- and freeze-onset dates derived from microwave satellite remote sensing.

In order to compare results from that parameterization with actual measurements presented in this study, we estimated the respective transmittance values according to the actual position and timing of each ROV station (Table 2). Results are compared against the mean transmittances observed during each ROV survey (Figure 9).

This shows that light transmittance values estimated by the parameterization do reproduce the correct seasonal cycle and correspond reasonably well to the ROV measurements. However, largest misfits are evident from late summer to autumn. This might be caused, on the one hand, by neglecting the bimodal distribution of light transmittance during autumn in the parameterization but using a strict decrease in light transmittance as soon as freezeup starts. On the other hand, we identified a misfit in sea ice classes between observations and parameterization toward more perennial sea ice in the latter case, leading to weaker light transmittance values than actually observed. Moreover, shown differences might be related to neglected variations in ice thickness for the given parameterizations.

In addition we compare with output from existing runs of a version of the MITgcm model that uses the parameterization of Grenfell and Maykut (1977) for calculation of under-ice light under both snow free and snow-covered sea ice. In this MITgcm configuration, the parameterization is evaluated separately for each of the seven ice and snow classes in the model, and the resulting under-ice light is the average value for each grid cell (Castellani et al., 2017). Available model output only covers the years of 2011 and 2012 of our data set. Figure 9 shows clearly, that the model cannot reproduce the large light transmittances during August and September associated with melt pond cover, but in turn overestimates light transmittance in autumn. This is likely caused by the inaccurate description of surface properties in the model, which does not feature melt ponds or a precise representation of snow layers.

In a next step, the described unique data set of light transmittance values of Arctic sea ice can be used to evaluate large-scale parameterizations. Doing so, we use the described parameterization by Arndt and Nicolaus (2014, AN14) as well as the one from Grenfell and Maykut (1977), both based on local measured geometry (GM77) as well as from the modified MITgcm model output (Castellani et al., 2017, C17). Figure 10 shows scatterplots of both parameterizations compared to station averages and individual measurements, respectively. While data points scatter on both sides of the diagonal in the AN14 and GM77 comparison, in a vast majority of cases the parameterizations overestimate light transmittance (77% for GM77 and 56 % for AN14). For C17, modeled light transmittance is mostly severely underestimated likely due to a lacking

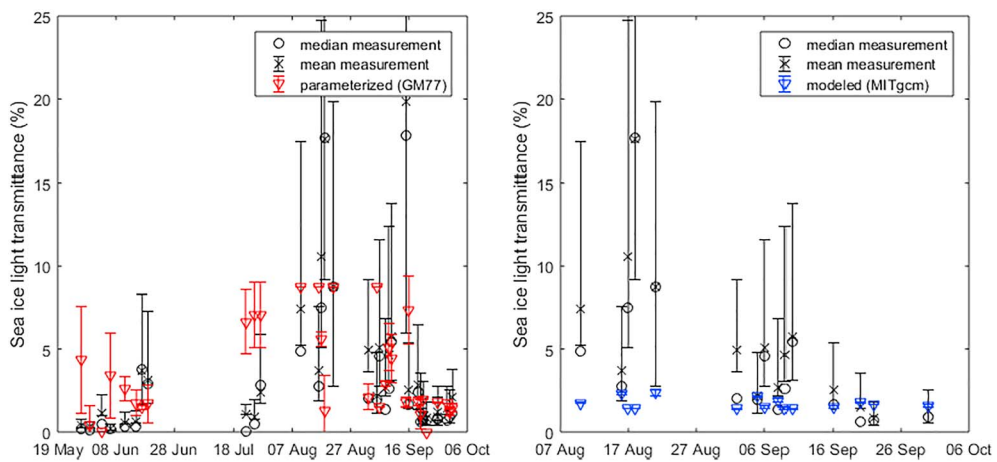


Figure 9. Comparison of measured mean transmittances to the parameterization of Arndt and Nicolaus (2014; left) and to model results from runs with the MITgcm configuration of Castellani et al. (2017). Black error bars indicate the 25% and 75% quartiles of remotely operated vehicle-measured transmittance, while colored error bars are the standard deviation of nine adjacent grid cells surrounding the station's position. Mind the different temporal range of both comparisons due to limited availability of model output.

representation of summer surface features and melt ponds. Even though, the overestimation by GM77 derived from local measured ice geometry is unexpected as it neglects any melt pond influence on the prevalent light transmittance, it is consistent with our retrieval of bulk extinction coefficients higher than the regularly used values. This also reflects the presence of snow or surface scattering layers in our data set that is not accounted for in the formulation of this parameterization. Thus, this explicit parameterization used in large-scale ice-ocean models, might overestimate light transmittance, especially in situations where snow or surface scattering layers are present, while it clearly fails to consistently represent the high light transmittances caused by ponded ice surfaces. The general scatter in point derived transmittances (GM77) is quite large with a transmittance root-mean-square error (RMSE) of 9.6%. For station averages the RMSE is however only 5.07% consistent with the other two approaches. For the Arndt and Nicolaus (2014) large-scale parameterization, which ignores actual sea ice geometry but rather focuses on seasonal sea ice surface and ice type variations, the RMSE of 5.05% is very similar, despite the completely different approach. This reveals, that on a basin-wide scale, these parameters are a

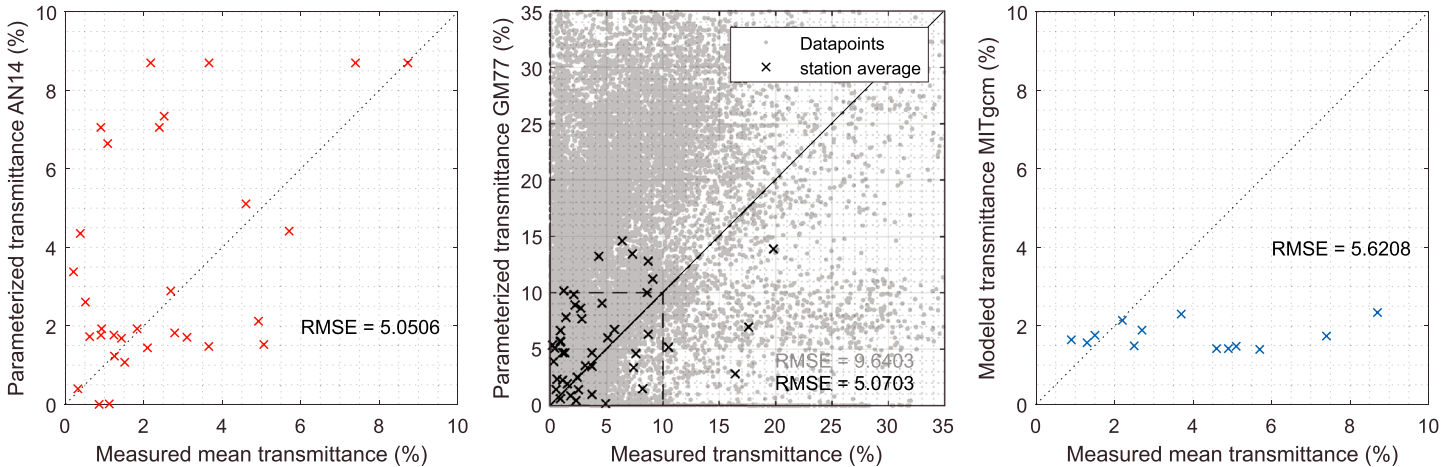


Figure 10. Scatterplots of parameterized and measured light transmittance: The left panel shows mean station transmittances in comparison to the parameterization of Arndt and Nicolaus (2014). The center panel provides a similar comparison, but on the individual measurements using the parameterization presented by (Grenfell & Maykut, 1977). Gray dots represent comparison of individual remotely operated vehicle point measurements, while black crosses indicate station averages. The dashed square indicates the different ranges of transmittance covered by methods shown in the other two panels. The right panel shows mean station transmittances in comparison to the MITgcm model results from Castellani et al. (2017).

much more important and capable predictor of optical sea ice properties than ice thickness alone. Evaluating the C17 results reveals an RSME of 5.6% in comparison to our observations. Thus, either a detailed geometric description with exact properties of the melting surface layers or some seasonally dependent additional information will be necessary for any successful parameterization of radiative transfer in sea ice.

4.4. Limitations

Our study describes the light transmittance through solid sea ice floes that are large and thick enough to provide a safe working environment. While this is certainly representative of most floes within the inner Arctic pack ice, smaller and more vulnerable ice floes in the marginal ice zone are not included in our study. Also, other ice types that are hard to access, such as brash ice or refrozen leads, are largely underrepresented in our data set. To cover the appropriate portions of this variability, future missions with longer range conducted by, for example, autonomous underwater vehicles are necessary.

Any attempt of upscaling the presented sea ice light transmittance observations to a regional under-ice light-climate will need to take into account the effect of ice concentration. Open water between single floes remains the most translucent window for sunlight to enter the upper ocean during summer, even when a significant melt pond cover is present.

As indicated above, this pseudo time series is not a strict time series in the classical sense. Differences between stations arise from many other factors, such as regional and interannual differences in melt progression or ice thickness as well as snow thickness variations driven by large-scale synoptic atmospheric and oceanic forcing. The results thus have to be interpreted with care on a larger-scale without singling out individual stations. Nevertheless, a careful interpretation of this comprehensive compilation of over 5 years of data from under-ice ROV observations can be used to derive the presented qualitative picture of the seasonal progression of the spatially varying light transmission through sea ice. While the classical time series observations from drifting buoys presented in this study suffer from a lack of information about the spatial variability, the combination with our spatially extensive ROV observations allows us to derive a rough but consistent picture.

5. Summary and Conclusions

Here, we presented a large data set of spatially distributed light transmittance measurements covering the complete cycle from the beginning of the melt season until freezeup. Measurements were obtained with an ROV and are located at numerous ice station locations along six cruise tracks of icebreaker expeditions in the Eurasian and Central Arctic.

Beyond the confirmation of typical features of the seasonal evolution of light transmission described in previous studies, our data set provides a comprehensive view on the development of spatial variability of ice optical properties and how light transmittance histograms are influenced by surface features, ice structures and the seasonal progression. During melting, the light transmittance histogram widens and develops a bimodal structure with the onset of pond formation. This bimodal structure is kept throughout the summer even until several weeks after freezeup when the total transmittance is decreasing again until significant snow fall renders the ice cover opaque. Our data set of hyperspectral measurements also suggests that decreased early summer light transmission through sea ice moderated by sea ice algae might be a widespread feature in the Arctic.

The large data set allowed us to assess three different light transmittance parameterizations, including one that has been frequently used in coupled ice-ocean models. Our results comparing these parameterizations with ROV measurements indicate that light transmission might be overestimated especially during late spring and early autumn in many cases. This is likely caused by the very simplified treatment of the sea ice surface—for example a fixed value of i_0 —as the historical point measurements used to derive the parameterization do not include a wide variety of sea ice variability including factors such as algal content, surface scattering layers, or even occasional thin snow cover. Furthermore, the parameterization is frequently used beyond the boundaries for which it had been originally designed for.

We therefore suggest that parameters in large-scale parameterizations for light transmittance on snow free unponded sea ice should be adjusted toward lower light transmittance to achieve a more realistic under-ice light field and present a potential parameterization that might be used when keeping the conceptual framework. However, we want to stress, that any future successful parameterization of light transfer in large-scale

models needs to explicitly include a dedicated treatment of surface properties to represent the changing surface consisting of snow, surface scattering layers and melt ponds. Also, we want to highlight that extinction parameters cannot be transferred between different model geometries and care must be taken when choosing parameters for large-scale parameterizations on the basis of only point measurements.

In general, we have shown that our large data set can be used to improve the understanding of representativeness of existing parameterizations and develop new improved parameterizations.

Acknowledgments

We gratefully acknowledge the support of Chief Scientists Ursula Schauer, Antje Boetius, Ilka Peeken, Andreas Macke, Hauke Flores, and the Captains and Crew of R/V *Polarstern* expeditions ARK-XXVI/3, ARK-XXVI/3, PS86 (AWI_PS86_00), PS92 (AWI_PS92_00), PS101 (AWI_PS101_00), and PS106 (AWI_PS106_00). Nereid-UI development and at-sea operations were supported by the U.S. National Science Foundation Office of Polar Programs (NSF OPP ANT-1126311), National Oceanic and Atmospheric Administration Office of Exploration and Research (NOAA OER NA14OAR4320158), the Woods Hole Oceanographic Institution, the James Family Foundation, and the George Frederick Jewett Foundation East. Additional funds supporting the ROV work in 2012 were provided to Antje Boetius by the European Research Council Advanced Investigator Grant 294757. The position of C. K. as well as the development of the BEAST ROV used in 2016 and 2017 were funded by the Helmholtz Infrastructure Initiative “Frontiers in Arctic Marine Monitoring (FRAM).” Writing of this manuscript was also supported by a Sentinel North postdoctoral fellowship at Université Laval (Quebec) to C. K. This study was funded by the Alfred-Wegener-Institut Helmholtz-Zentrum für Polar- und Meeresforschung. The reprocessed and quality controlled data set created for this publication is accessible at <https://doi.pangaea.de/10.1594/PANGAEA.896219>.

References

- Arndt, S., Meiners, K. M., Ricker, R., Krumpen, T., Katlein, C., & Nicolaus, M. (2017). Influence of snow depth and surface flooding on light transmission through Antarctic pack ice. *Journal of Geophysical Research: Oceans*, 122, 2108–2119. <https://doi.org/10.1002/2016JC012325>
- Arndt, S., & Nicolaus, M. (2014). Seasonal cycle and long-term trend of solar energy fluxes through Arctic sea ice. *The Cryosphere*, 8(6), 2219–2233. <https://doi.org/10.5194/tc-8-2219-2014>
- Arrigo, K. R., Perovich, D. K., Pickart, R. S., Brown, Z. W., van Dijken, G. L., Lowry, K. E., et al. (2012). Massive phytoplankton blooms under Arctic sea ice. *Science*, 336(6087), 1408–1408. <https://doi.org/10.1126/science.1215065>
- Assmy, P., Fernández-Méndez, M., Duarte, P., Meyer, A., Randelhoff, A., Mundy, C. J., et al. (2017). Leads in Arctic pack ice enable early phytoplankton blooms below snow-covered sea ice. *Scientific reports*, 7(1), 40850. <https://doi.org/10.1038/srep40850>
- Boetius, A. (2013). *The expedition of the research vessel “Polarstern” to the Arctic in 2012 (ARK-XXVII/3 - IceArc)Rep.* Bremerhaven: Alfred Wegener-Institut.
- Boetius, A. (2015). *The expedition PS86 of the research vessel POLARSTERN to the Arctic Ocean in 2014*, edited. Bremerhaven: Alfred Wegener Institute for Polar and Marine Research.
- Boetius, A., & Purser, A. (2017). *The Expedition PS101 of the Research Vessel POLARSTERN to the Arctic Ocean in 2016*, edited. Bremerhaven: Alfred Wegener Institute for Polar and Marine Research.
- Briegleb, B. P., & Light, B. (2007). A delta-Eddington multiple scattering parameterization for solar radiation in the sea ice component of the Community Climate System Model,. *NCAR Technical Note*. <https://doi:10.5065/D6B27S71>
- Castellani, G., Losch, M., Lange, B. A., & Flores, H. (2017). Modeling Arctic sea-ice algae: Physical drivers of spatial distribution and algae phenology. *Journal of Geophysical Research: Oceans*, 122, 7466–7487. <https://doi.org/10.1002/2017JC012828>
- Castro-Morales, K., Kauker, F., Losch, M., Hendricks, S., Riemann-Campe, K., & Gerdes, R. (2014). Sensitivity of simulated Arctic sea ice to realistic ice thickness distributions and snow parameterizations. *Journal of Geophysical Research: Oceans*, 119, 559–571. <https://doi.org/10.1002/2013JC009342>
- Ehn, J. K., Papakyriakou, T. N., & Barber, D. G. (2008). Inference of optical properties from radiation profiles within melting landfast sea ice. *Journal of Geophysical Research*, 113, C09024. <https://doi.org/10.1029/2007JC004656>
- Fernández-Méndez, M., Rabe, B., Katlein, C., Nicolaus, M., & Boetius, A. (2015). Central Arctic primary production and its limiting factors during the sea ice extent minimum record year 2012. *Biogeosciences*, 12(11), 3525–3549. <https://doi.org/10.5194/bg-12-3525-2015>
- Fetterer, F., & Untersteiner, N. (1998). Observations of melt ponds on Arctic sea ice. *Journal of Geophysical Research*, 103(C11), 24,821–24,835. <https://doi.org/10.1029/98JC02034>
- Flocco, D., Feltham, D. L., Bailey, E., & Schroeder, D. (2015). The refreezing of melt ponds on Arctic sea ice. *Journal of Geophysical Research: Oceans*, 120, 647–659. <https://doi.org/10.1002/2014JC010140>
- Grenfell, T. C., Light, B., & Perovich, D. K. (2006). Spectral transmission and implications for the partitioning of shortwave radiation in arctic sea ice. In P. Langhorne & V. Squire (Eds.), *Annals of Glaciology* (Vol. 44, 2006, pp. 1–6). Cambridge: Int Glaciological Soc. <https://doi.org/10.3189/172756406781811763>
- Grenfell, T. C., & Maykut, G. A. (1977). The optical properties of ice and snow in the arctic basin. *Journal of Glaciology*, 18(80), 445–463. <https://doi.org/10.1017/S0022143000021122>
- Grenfell, T. C., & Perovich, D. K. (1981). Radiation absorption coefficients of polycrystalline ice from 400–1400 nm. *Journal of Geophysical Research*, 86(NC8), 7447–7450. <https://doi.org/10.1029/JC086iC08p7447>
- Haas, C., Pfaffling, A., Hendricks, S., Rabenstein, L., Etienne, J.-L., & Rigor, I. (2008). Reduced ice thickness in Arctic Transpolar Drift favors rapid ice retreat. *Geophysical Research Letters*, 35, L17501. <https://doi.org/10.1029/2008GL034457>
- Holland, M. M., Bailey, D. A., Briegleb, B. P., Light, B., & Hunke, E. (2011). Improved sea ice shortwave radiation physics in CCSM4: The impact of melt ponds and aerosols on Arctic sea ice. *Journal of Climate*, 25(5), 1413–1430. <https://doi.org/10.1175/JCLI-D-11-00078.1>
- Katlein, C., Arndt, S., Nicolaus, M., Perovich, D. K., Jakuba, M. V., Suman, S., et al. (2015). Influence of ice thickness and surface properties on light transmission through Arctic sea ice. *Journal of Geophysical Research: Oceans*, 120, 5932–5944. <https://doi.org/10.1002/2015JC010914>
- Katlein, C., Fernández-Méndez, M., Wenzhöfer, F., & Nicolaus, M. (2014). Distribution of algal aggregates under summer sea ice in the Central Arctic. *Polar Biology*, 38(5), 719–731. <https://doi.org/10.1007/s00300-014-1634-3>
- Katlein, C., Perovich, D. K., & Nicolaus, M. (2016). Geometric effects of an inhomogeneous sea ice cover on the under ice light field. *Frontiers in Earth Science*, 4. <https://doi.org/10.3389/feart.2016.00006>
- Katlein, C., Schiller, M., Belter, H. J., Coppolaro, V., Wenslandt, D., & Nicolaus, M. (2017). A new remotely operated sensor platform for interdisciplinary observations under sea ice. *Frontiers in Marine Science*, 4(281). <https://doi.org/10.3389/fmars.2017.00281>
- Lee, S. H., McRoy, C. P., Joo, H. M., Gradinger, R., Cui, H., Yun, M. S., et al. (2011). Holes in progressively thinning Arctic sea ice lead to new ice alga habitat. *Oceanography*, 24(3), 302–308. <https://doi.org/10.5670/oceanog.2011.81>
- Light, B., Grenfell, T. C., & Perovich, D. K. (2008). Transmission and absorption of solar radiation by Arctic sea ice during the melt season. *Journal of Geophysical Research*, 113, C03023. <https://doi.org/10.1029/2006JC003977>
- Light, B., Maykut, G. A., & Grenfell, T. C. (2003). A two-dimensional Monte Carlo model of radiative transfer in sea ice. *Journal of Geophysical Research*, 108(C7), 3219. <https://doi.org/10.1029/2002JC001513>
- Light, B., Perovich, D. K., Webster, M. A., Polashenski, C., & Dadic, R. (2015). Optical properties of melting first-year Arctic sea ice. *Journal of Geophysical Research: Oceans*, 120, 7657–7675. <https://doi.org/10.1002/2015JC011163>

- Liu, J., Zhang, Z., Inoue, J., & Horton, R. M. (2007). Evaluation of snow/ice albedo parameterizations and their impacts on sea ice simulations. *International Journal of Climatology*, 27(1), 81–91. <https://doi.org/10.1002/joc.1373>
- Losch, M., Menemenlis, D., Campin, J.-M., Heimbach, P., & Hill, C. (2010). On the formulation of sea-ice models. Part 1: Effects of different solver implementations and parameterizations. *Ocean Modelling*, 33(1–2), 129–144. <https://doi.org/10.1016/j.ocemod.2009.12.008>
- Macke, A., & Flores, H. (2018). *The Expeditions PS106/1 and 2 of the Research vessel POLARSTERN to the Arctic Ocean in 2017*, edited. Bremerhaven: Alfred Wegener Institute for Polar and Marine Research. https://doi.org/10.2312/BzPM_0719_2018
- Marshall, J., Adcroft, A., Hill, C., Perelman, L., & Heisey, C. (1997). A finite-volume, incompressible Navier Stokes model for studies of the ocean on parallel computers. *Journal of Geophysical Research*, 102(C3), 5753–5766. <https://doi.org/10.1029/96JC02775>
- Maslanik, J. A., Fowler, C., Stroeve, J., Drobot, S., Zwally, J., Yi, D., & Emery, W. (2007). A younger, thinner Arctic ice cover: Increased potential for rapid, extensive sea-ice loss. *Geophysical Research Letters*, 34, L24501. <https://doi.org/10.1029/2007GL032043>
- Meier, W. N., Hovelsrud, G. K., van Oort, B. E. H., Key, J. R., Kovacs, K. M., Michel, C., et al. (2014). Arctic sea ice in transformation: A review of recent observed changes and impacts on biology and human activity. *Review of Geophysics*, 52, 185–217. <https://doi.org/10.1002/2013RG000431>
- Mobley, C. D., Cota, G. F., Grenfell, T. C., Maffione, R. A., Pegau, W. S., & Perovich, D. K. (1998). Modeling light propagation in sea ice. *IEEE Transactions on Geoscience and Remote Sensing*, 36(5), 1743–1749. <https://doi.org/10.1109/36.718642>
- Nicolaus, M., Gerland, S., Hudson, S. R., Hanson, S., Haapala, J., & Perovich, D. K. (2010). Seasonality of spectral albedo and transmittance as observed in the Arctic Transpolar Drift in 2007. *Journal of Geophysical Research*, 115, C11011. <https://doi.org/10.1029/2009JC006074>
- Nicolaus, M., Hudson, S. R., Gerland, S., & Munderloh, K. (2010). A modern concept for autonomous and continuous measurements of spectral albedo and transmittance of sea ice. *Cold Regions Science and Technology*, 62(1), 14–28. <https://doi.org/10.1016/j.coldregions.2010.03.001>
- Nicolaus, M., & Kattlein, C. (2013). Mapping radiation transfer through sea ice using a remotely operated vehicle (ROV). *The Cryosphere*, 7(3), 763–777. <https://doi.org/10.5194/tc-7-763-2013>
- Nicolaus, M., Kattlein, C., Maslanik, J., & Hendricks, S. (2012). Changes in Arctic sea ice result in increasing light transmittance and absorption. *Geophysical Research Letters*, 39, L24501. <https://doi.org/10.1029/2012GL053738>
- Nicolaus, M., Petrich, C., Hudson, S. R., & Granskog, M. A. (2013). Variability of light transmission through Arctic land-fast sea ice during spring. *The Cryosphere*, 6(5), 4363–4385. <https://doi.org/10.5194/tcd-6-4363-2012>
- Peeken, I. (2016). *The Expedition PS92 of the Research vessel POLARSTERN to the Arctic Ocean in 2015*, edited. Bremerhaven: Alfred Wegener Institute for Polar and Marine Research.
- Perovich, D. K. (1990). Theoretical estimates of light reflection and transmission by spatially complex and temporally varying sea ice covers. *Journal of Geophysical Research*, 95(C6), 9557–9567. <https://doi.org/10.1029/JC095iC06p09557>
- Perovich, D. K. (1996). The optical properties of sea ice, Monograph 96-1.
- Perovich, D. K., Grenfell, T. C., Light, B., & Hobbs, P. V. (2002). Seasonal evolution of the albedo of multiyear Arctic sea ice. *Journal of Geophysical Research*, 107(C10), 8044. <https://doi.org/10.1029/2000JC000438>
- Perovich, D. K., Jones, K. F., Light, B., Eicken, H., Markus, T., Stroeve, J., & Lindsay, R. (2011). Solar partitioning in a changing Arctic sea-ice cover. *Annals of Glaciology*, 52(57), 192–196. <https://doi.org/10.3189/172756411795931543>
- Perovich, D. K., Light, B., Eicken, H., Jones, K. F., Runciman, K., & Nghiem, S. V. (2007). Increasing solar heating of the Arctic Ocean and adjacent seas, 1979–2005: Attribution and role in the ice-albedo feedback. *Geophysical Research Letters*, 34, L19505. <https://doi.org/10.1029/2007GL031480>
- Perovich, D. K., Longacre, J., Barber, D. G., Maffione, R. A., Cota, G. F., Mobley, C. D., et al. (1998). Field observations of the electromagnetic properties of first-year sea ice, *Geoscience and Remote Sensing. IEEE Transactions on*, 36(5), 1705–1715. <https://doi.org/10.1109/36.718639>
- Perovich, D. K., & Polashenski, C. (2012). Albedo evolution of seasonal Arctic sea ice. *Geophysical Research Letters*, 39, L08501. <https://doi.org/10.1029/2012GL051432>
- Perovich, D. K., Polashenski, C., Arntsen, A., & Swertka, C. (2017). Anatomy of a late spring snowfall on sea ice. *Geophysical Research Letters*, 44, 2802–2809. <https://doi.org/10.1002/2016GL071470>
- Polashenski, C., Perovich, D., & Courville, Z. (2012). The mechanisms of sea ice melt pond formation and evolution. *Journal of Geophysical Research*, 117, C01001. <https://doi.org/10.1029/2011JC007231>
- Renner, A. H. H., Gerland, S., Haas, C., Spreen, G., Beckers, J. F., Hansen, E., et al. (2014). Evidence of Arctic sea ice thinning from direct observations. *Geophysical Research Letters*, 41, 5029–5036. <https://doi.org/10.1002/2014GL060369>
- Schauer, U. (2012). *The expedition ARKTIS-XXVI/3 of the research vessel "Polarstern" in 2011*, edited, (p. 271). Bremerhaven: Alfred Wegener Institute for Polar and Marine Research.
- Schröder, D., Feltham, D. L., Flocco, D., & Tsamados, M. (2014). September Arctic sea-ice minimum predicted by spring melt-pond fraction. *Nature Climate Change*, 4(5), 353–357. <https://doi.org/10.1038/nclimate2203>
- Steele, M., Zhang, J., & Ermold, W. (2010). Mechanisms of summertime upper Arctic Ocean warming and the effect on sea ice melt. *Journal of Geophysical Research*, 115, C11004. <https://doi.org/10.1029/2009JC005849>
- Taylor, P. D., & Feltham, D. L. (2004). A model of melt pond evolution on sea ice. *Journal of Geophysical Research*, 109, C12007. <https://doi.org/10.1029/2004JC002361>
- Wang, C., Granskog, M. A., Gerland, S., Hudson, S. R., Perovich, D. K., Nicolaus, M., et al. (2014). Autonomous observations of solar energy partitioning in first-year sea ice in the Arctic Basin. *Journal of Geophysical Research: Oceans*, 119, 2066–2080. <https://doi.org/10.1002/2013JC009459>
- Wang, Q., Danilov, S., Sidorenko, D., Timmermann, R., Wekerle, C., Wang, X., et al. (2014). The Finite Element Sea Ice-Ocean Model (FESOM) v1.4: Formulation of an ocean general circulation model. *Geoscientific Model Development*, 7(2), 663–693. <https://doi.org/10.5194/gmd-7-663-2014>
- Webster, M. A., Rigor, I. G., Perovich, D. K., Richter-Menge, J. A., Polashenski, C. M., & Light, B. (2015). Seasonal evolution of melt ponds on Arctic sea ice. *Journal of Geophysical Research: Oceans*, 120, 5968–5982. <https://doi.org/10.1002/2015JC011030>
- Zhang, J., & Rothrock, D. A. (2003). Modeling global sea ice with a thickness and enthalpy distribution model in generalized curvilinear coordinates. *Monthly Weather Review*, 131(5), 845–861. [https://doi.org/10.1175/1520-0493\(2003\)131<0845:mgsiwa>2.0.co;2](https://doi.org/10.1175/1520-0493(2003)131<0845:mgsiwa>2.0.co;2)